RESEARCH ARTICLE

JOURNAL OF Applied Polymer **WILEY**
SCIENCE

Investigating the changing dynamics of processing, temperature-based mechanics, and flame retardancy in the transfer of ammonium polyphosphate/inorganic silicate flame retardants from epoxy resins to glass fiber composites

Sruthi Sunder[1] | Maria Jauregui Rozo[2] | Sneha Inasu[1] | Bernhard Schartel[2] |
Holger Ruckdäschel[1]

[1]Bundesanstalt für Materialforschung und-prüfung (BAM), Berlin, Germany

[2]Department Polymer Engineering, University of Bayreuth, Bayreuth, Germany

Correspondence
Sruthi Sunder and Holger Ruckdäschel, Bundesanstalt für Materialforschung und-prüfung (BAM), Unter den Eichen 87, 12205 Berlin, Germany.
Email: sruthi.sunder@uni-bayreuth.de and holger.ruckdaeschel@uni-bayreuth.de

Maria Jauregui Rozo and Bernhard Schartel, Department Polymer Engineering, University of Bayreuth, Universitätsstraße 30, 95447 Bayreuth, Germany.
Email: maria.jauregui@bam.de and bernhard.schartel@bam.de

Abstract

Although numerous investigations study the improvement of flame retardancy of epoxy resins using additives, maintaining the flame retardant (FRs) modes of action present in the resins upon transfer to composites is challenging. In this study, ammonium polyphosphate (APP) and inorganic silicate (InSi) are loaded at 10%, 30%, and 50% by weight, in a diglycidyl ether of bisphenol A (DGEBA) resin cured with dicyandiamide and transferred to bidirectional (BD) glass fiber (GF) composites. Although a 50% loading of the FRs impacts the curing kinetics of the resin system, the effect on the glass transition temperature of the resin system remains negligible compared to reactive FRs in the state of the art integrated into the resin's chemical structure. Increasing the FR content improved the heat release characteristics in both the resins and composites. However, the charring mode of action is completely suppressed in the formulation with 10% APP + InSi. A 30% concentration of the FRs restored the charring action in the composite and the GFs provide increased protective layer action upon transfer to the composites. This study highlights the importance of accounting for the changing dynamics related to processing and flame retardancy upon transferring FRs from resins to composites.

KEYWORDS
composites, flame retardance, resins, synthesis and processing techniques

1 | INTRODUCTION

Epoxy (EP) resins and their fiber reinforced composites are recognized for their versatility in their applications ranging from their use in electronic products, to

Sruthi Sunder and Maria Jauregui Rozo contributed equally to this work.

components for the construction, and transport sector.[1] Notwithstanding their exceptional mechanical properties which can be further enhanced via the use of glass fiber (GF) reinforcements,[2] and chemical resistance,[3–5] EP's inherent flammability[6,7] is a disadvantage. Such a challenge can be overcome with the use of flame retardant (FR) additives, prioritizing halogen-free options due to environmental and toxicity concerns.[8–12] Here, the use of intumescents such as ammonium polyphosphate (APP) not only effectively substitutes for halogenated FRs, but poses an additional advantage over other commonly used FR additives such as ATH or aluminum diethyl phosphinate (AldiP) where a temperature stability above 220°C, and where potentially higher char formation ability at loadings up to 50% w/w are prioritized.[13,14] In particular, the use of intumescent FRs in combination with other active FR additives such as alumina trihydrate or melamine cyanurate[15–18] reflects a successful strategy to reduce flammability in EP resins while minimizing smoke and toxic gas production during combustion. APP is known to produce charred structures in various polymers above 250°C due to dehydration following the release of ammonia and polyphosphoric acid.[19] Such a low-density charred structure can be further compacted and stabilized via additional components such as nanosilica[20] or low melting glasses such as inorganic silicates (InSi).[21,22] Wu et al.[22] examined the impact of incorporating InSi into a layered EP-clay composite. They found that combining InSi after refinement with APP in a ratio of 8:2, totaling 10% w/w in an EP resin system, was most effective at establishing a robust fire barrier. In order to avoid additional processing steps as explained by Liu et al.[21] in the refinement of the InSi structures, this investigation makes use of commercially available InSi with a narrower particle size distribution. In the past decades, considerable effort has been invested in the research and development of halogen-free synergistic FR combinations for unreinforced resin systems. Often, the most promising resin mixtures are then transferred to the fiber composite. This procedure saves time during development. For example, Zhang et al.[23] focused on improving the interaction between APP and the EP resin matrix, potentially through hydrophobic modification. Shao et al. performed a similar study by synthesizing a zeolitic imidazolate framework on the APP.[24] In another study by Yang et al.,[25] boron-containing FR APP was developed to enhance the fire resistance and impact toughness of EP resin. The high costs and effort involved in such chemically tailored structures hinders their transfer to composites on a production scale. It is unclear in these investigations whether the proposed FR additives are additionally sufficiently tailored for the composite. The reinforcing fibers are in direct contact with the

degradation products after burning, causing changes to the physical properties of the composite and the fire residue. Consequently, the FR properties as well as the formation of the fire residues may be enhanced or hindered. For instance, findings by Rajaei et al.[26] indicate improved flame retardancy via the incorporation of melamine-coated APP with talc in a diglycidyl ether of bisphenol A (DGEBA) resin and GF reinforced composites (GFRCs) at 30% w/w. However, in the case of the composites, the improvement in the heat release rate (HRR) is contrasted by a lowered UL-94 rating in the composites. In contrast, a study by Lim et al.[17] showed that a V-0 rating attained by adding ~10% w/w APP to a modified EP resin for highly filled systems, was maintained upon transfer to GFRCs. It is difficult to accurately ascertain that the improvement in flame retardancy can truly be attributed to the presence of the FRs in the case of the composites. The effectiveness of the FRs in reducing overall flammability may be overpowered by the thermally inert[27] GFs in the resin, which may contrastingly cause a change in the melt flow, dripping, or a candlewick effect[28] that lowers the UL-94 rating of a composite. Such effects are more evident in intumescent systems where the potency of the FR effect depends heavily on maintaining a specific viscosity during burning, and where adding mechanical reinforcement might completely hinder their intumescent ability.[29] Although several investigations delve into the fire performance of the relevant FR systems in the resins, limited consideration is given to the rheological behavior, curing kinetics, and temperature-based mechanics of the systems prior to fire testing. Moreover, insufficient attention is given to quantifying the varying modes of action of the FRs upon transfer from resins to composites. Hu et al., Rabe et al.,[30] and Brehme et al.[30–32] previously addressed techniques to quantify the charring mechanisms, reduction in apparent effective heat of combustion (EHC) and protective layer mechanisms relative to a defined reference system in various FR thermoplastic systems. These mechanisms are chosen due to their importance in indicating the prevention of flame spread and propagation in the gas or condensed phases via barrier formation, flame inhibition, fuel dilution, or endothermic heat sink formation. Here, condensed phase mechanisms such as, charring or barrier formation as in the case of intumescents such as APP, can prevent oxygen access to the surface or fuel release from the surface of the polymer leading to effective flame spread prevention. Dehydration reactions such as those occurring with ATH that cause the release of water and cause a cooling effect via an endothermic heat sink, effectively diluting the heat of the flame. Moreover, gas phase mechanisms such as those found in the release of ammonia upon the degradation of APP can cause flame dilution, effectively

preventing flame spread. In this regard, the transfer of these FR formulations and their modes of action to GF-reinforced EP composites requires additional consideration. The complexity of interactions between the FR additives, resin matrix and the GF reinforcement means that predicting the successful transfer of these modes of action is challenging without suitable quantitative verification.[33]

Previous work by Sunder and Jauregui Rozo et al.[34] has already shown that APP, melamine polyphosphate (MPP) as well as silane coated APP in combination with InSi loaded at 10% w/w in EP resins do not retain their fire residue formation ability upon transfer to GF reinforced composites with both uniaxial and biaxial textile architectures. The composites containing 10% w/w APP + InSi in the resin yielded more reliable fiber volume contents of ~57%–60% compared to those containing MPP or Si-APP. Based on the existing literature, the first identifiable research gap in the current state of the art is that the transfer of these formulations to composites is not explicitly studied. A second identifiable research gap in the state of the art that arises here, is the lack of quantified data on the transferability of FR modes of action from resins to composites, especially with higher relative fiber weight contents above 70%. Thus, this study concentrates on understanding the changing dynamics of flame retardancy and processing in the transition from resin to composite, addressing a crucial aspect in the field of composite material development for high-performance applications. Systematic consideration is given to the processing parameters as well as to the temperature-based mechanics of the systems prior to their transfer to the composites via rheology, differential scanning calorimetry (DSC), and dynamic mechanical thermal analysis (DMTA). The distribution of the additives within the composites was visualized using scanning electron microscopy (SEM). The fire performance of the resins and composites was compared using cone calorimeter measurements, LOI, and UL-94 tests and the modes of action of the FRs were quantified. The effect of increasing the combined APP + InSi content in the DGEBA resin via low filled (10% w/w), moderately filled (30% w/w), and highly filled (50% w/w) systems are comparatively investigated for transfer to bidirectional (BD) GFRCs via prepregs. Despite the atypical loading content, the highly filled system is investigated here to match the overall active P content of ~3% used in the resin upon transfer of the resin to the GFRC and to gauge the effects of upper loading limits to recover the modes of action of the FRs in the composite. Therefore, the FR modes of action are calculated and compared for the resins and composites for their charring, reduction in apparent EHC and protective layer mechanisms. The potential trade-offs due to additional loading of the FRs, and the mechanical behavior of these resins and composites pre- and post-fire, will be investigated in a separate study due to complex considerations involved in the study of the post-fire mechanics of the composites.

2 | EXPERIMENTAL SECTION

2.1 | Materials and methods

Figure 1 provides an overview of the materials, processing, and analysis methods used in this study.

2.1.1 | Resin and composite formulation and curing

DGEBA EP resin—DER 331 was obtained from Olin EP. The resin had an epoxy equivalent weight (EEW) of EEW: 182–192 g/eq, with a viscosity of 11–14 Pa s and a density of 1.16 g/cm^3 at room temperature. The resin was combined in a stoichiometric ratio of 100:6.5:1 with a dicyandiamide (DICY) hardener (DYHARD 100S/Alzchem) and an Urone accelerator (DYHARD UR400/Alzchem). Both the hardener and accelerator used had a d_{98}: <10 μm. The ratio of the resin:hardener:accelerator was chosen based on Equation 1:

$$PHR = \left[\frac{100 \times (AHEW_{curing\ agent})}{(EEW_{epoxy\ resin})} \right] \quad (1)$$

Where PHR indicates the quantity of the curing agent in parts per 100 added to the resin, and AHEW is the amine hydrogen equivalent weight of the curing agent. The combination of the DGEBA + DICY + Urone accelerator without additives will be referred to hereon simply as E100. Table 1 summarizes the various FR contents in the DGEBA resin, and the composites produced. APP (FR CROS 484/Budenheim) was combined with InSi (Flamtard V100/William Blythe) in the ratio of 8:2 for all formulations. The combined mixture had a $d_{90} \leq 30$ μm. Here, d_{90} signifies the size point below which 90% of the material is contained. The curing agents and FRs were evenly dispersed within the resin using a dual asymmetric centrifuge speed mixer (Hauschild Engineering). The mixing process took place for 2 min at a speed of 3000 rpm to ensure the homogeneity of the resin. Subsequently, the formulations underwent degassing at 15–20 mbar under vacuum for a minimum of 10 min to eliminate any trapped air introduced during mixing. The prepared mixture was then poured into molds of varying
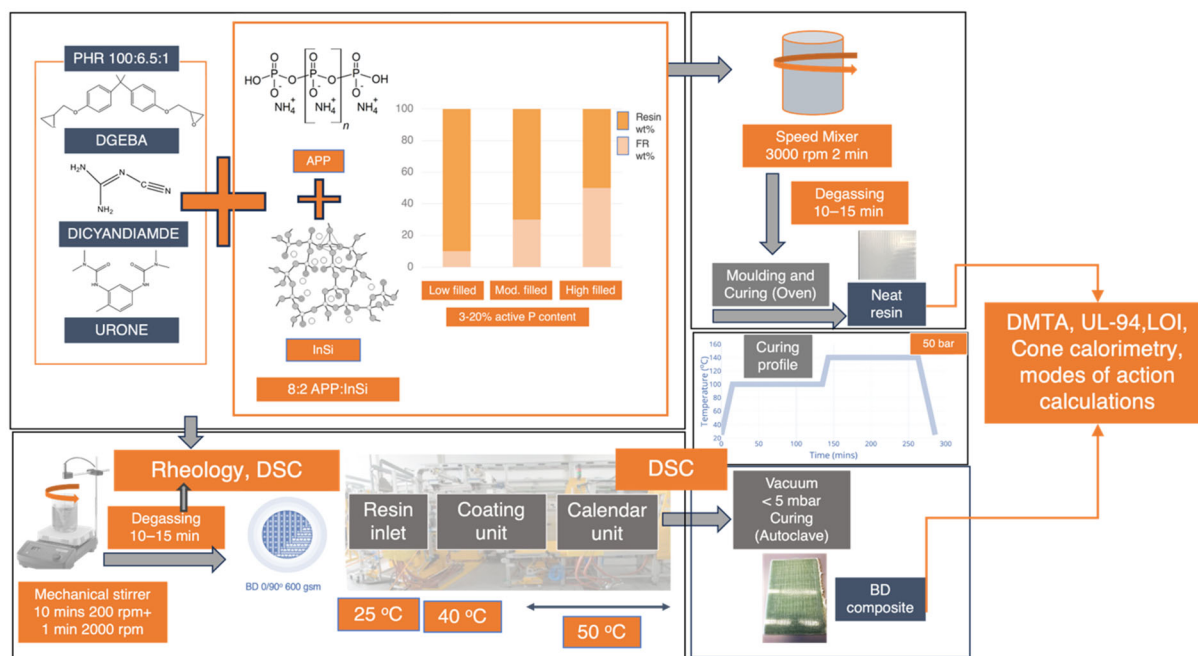
FIGURE 1 Overview of the materials, processing methods, and analyses conducted in this investigation. [Color figure can be viewed at wileyonlinelibrary.com]

TABLE 1 Summary of FR resin and composite formulations.

Sample label	Total active FR % Resin systems P	N	DGEBA + DICY + UR400 % wt	InSi % wt in resin	APP	GF:BD -
E100	0	0	100	0	0	-
E90InSi2APP8	3.75	1.3	90	2	8	-
E70InSi6APP24	11.25	3.9	70	6	24	-
E50InSi10APP40	18.75	6.5	50	10	40	-
Composites			% wt in composite	% wt in resin		% wt in composite
E100:GF-BD	0	0	27	0	0	73
E90InSi2APP8:GF-BD	0.1	0.0377	29 (incl. FRs)	2	8	71
E70InSi6APP24:GF-BD	1	0.864	30 (incl. FRs)	6	24	70
E50InSi10APP40:GF-BD	2.8	0.975	30 (incl. FRs)	10	40	70

Abbreviations: APP, ammonium polyphosphate; DGEBA, diglycidyl ether of bisphenol A; DICY, dicyandiamide; FR, flame retardant.

thicknesses, depending on the specific tests planned. The curing of these mixtures was carried out in a Memmert ULE 400 convection oven, manufactured by Memmert GmbH in Germany. The curing process involved an initial fixed ramp of 5°C per minute up to 100°C maintained for 2 h, followed by a second ramp-up to 140°C at a ramp rate of 5°C per min maintained for an additional 2 h. Following the curing process, the molds were allowed to cool overnight, resulting in the formation of EP resin

plates. The weight percent of the GFs was checked in-line during the prepreg manufacturing process. For all prepregs, BD layered glass fibers (BD GF) (G600BD-1300/ Saertex GmbH) with an aerial density of 600 g/m² were used. The resin mixtures were prepared using a mechanical stirrer where the formulations were mixed for 10 min at low speed (200 rpm) followed by 1–2 min at high speed (2000 rpm) for homogeneity. The construction of the fabric comprises E-glass of 1100 tex with a density of

346 g/m^2 in the 0° direction, E-glass 600 tex with a density of 283 g/m^2 in the 90° direction, and a backing yarn of polyethersulfone (110 dtex: 3 g/m^2). The prepregs were produced utilizing a laboratory scale prepreg line (EHA Composites Machinery). To prevent resin thinning, the resins were introduced to the coating unit at temperatures where their viscosity approaches 1000 mPa s through direct film coating on siliconized release paper, with a line speed of 1.5 m/min. In the calendar unit, the resins impregnated the glass fabrics, with the fabrics covered by siliconized paper. The resin was applied to a width of 220 mm on the 300 mm wide glass fabric, after which the material was rolled, vacuum sealed, and stored at $-18°C$. The fibers were supplied to the line in the 0° fiber orientation. The relevant temperatures used in the inlet, coating, and calendar unit are described further in the results from the rheology measurements.

The BD GF prepregs, measuring 220×300 mm, were manually layered, and stacked through hand layup onto a steel plate covered with a smooth laminating foil. Subsequently, these layers were vacuum bagged and subjected to curing in an autoclave setup under a pressure of 50 bars and under vacuum conditions (< 20 mbar), with no additional air pressure applied. The curing process involved a gradual temperature increase, commencing with an initial ramp to 100°C for 2 h, followed by a second ramp to 140°C for an additional 2 h, and finally, a cool-down ramp to room temperature over a minimum of 4 h. The ramp rates were constant at $\pm 5°C/\text{min}$.

The resulting laminate thicknesses for all composite formulations averaged 2.5 ± 0.3 mm when utilizing 5 layers of GFs, 3.2 ± 0.3 mm for 7 layers of GFs, and 4.4 ± 0.3 mm when employing 9 layers of GFs for the GFRCs.

2.2 | Processability of the resins and composites

2.2.1 | Rheology

The processability of FR combinations as additives for DGEBA systems was assessed using an Anton Paar Rheometer (MCR 301). The rheological characteristics of the uncured samples were then examined within the linear viscoelastic region, employing a parallel plate (PP25) with a 1 mm gap between the plates over the temperature range of 25–200°C, following a temperature ramp of 3°C/min. Complex viscosities of the resin formulations were tested to ensure that they are within the range of 10–50,000 mPa s in a processable temperature range, aligning with optimal prepreg processing conditions at the plant line.[35] These limits are the inherent technical operational ranges of the specified prepreg production machinery used in this study and are necessary for

ensuring optimal impregnation and processing of the prepregs. Additionally, frequency sweep measurements were performed ranging from 0.1 to 100 rad/s with a constant applied strain of 0.1% considering the linear viscoelastic region, at two constant temperatures of 50 and 100°C.

2.2.2 | Differential scanning calorimetry

The initiation of curing, full curing, and the enthalpy associated with the curing process were examined during the initial heating cycle through dynamic DSC measurements. A Mettler Toledo DSC 1 (Columbus), was employed for this analysis, utilizing a heating ramp rate of 10 K/min and a measurement range spanning from 25 to 275°C. The nitrogen flow rate was established at 50 mL/min, and a sample mass of 20 ± 2 mg was utilized. Two samples were tested per formulation.

2.2.3 | Dynamic mechanical thermal analysis

DMTA was conducted on a Gabo Eplexor 500 N to examine the properties of unreinforced resin, as well as BD composite samples, both below and above the glass transition temperature (T_g). Torsion mode measurements were performed on specimens with dimensions of 50 mm x 10 mm x 2 mm, utilizing a temperature range from 25 to 180°C with a temperature ramp of 3 K/min. The glass transition temperature (T_g) was identified by determining the peak of the loss factor (tan δ). Each sample type was tested with three specimens.

2.2.4 | Composite morphology

The cured surfaces of the composite samples were cut to size (1 mm $\times$ 2 mm) and embedded in a DGEBA EP resin and hardener using embedding springs (EpoFix-Struers) for visualization were analyzed using a Zeiss Gemini 1530 Scanning Electron Microscope from Carl Zeiss AG. The sample surfaces were sputtered using platinum up to a thickness of 5 nm. An acceleration voltage of 3 kV was used.

2.3 | Fire performance of the resins and composites

2.3.1 | Cone calorimetry

All specimens, sized at 100 mm $\times$ 100 mm $\times$ 4 mm, were assessed in a horizontal orientation under an

external heat flux of 50 kWm^{-2} following ISO 5660-1 guidelines, using a Dual Cone Calorimeter from Fire Testing Technology Ltd. in East Grinstead, UK. To avert any interference with the cone heater, the distance between the sample and the heat source was adjusted to 35 mm instead of 25 mm.[36] Prior to conducting the measurements, the samples were conditioned at 23°C and 50% relative humidity for a minimum of 5 days.

2.3.2 | Flammability testing

The flammability assessment of the specimens involved the vertical and horizontal UL-94 tests (Underwriter's Laboratory), in accordance with IEC 60695–11-10, and the limited oxygen index (LOI) following ISO 4589-2. For the UL-94 test, the specimen dimensions were 125 mm × 13 mm × 3 mm, while for LOI determination, the dimensions were 130 mm × 6.5 mm × 3 mm. In cases where samples did not meet the criteria in the vertical test, they underwent evaluation in the horizontal test. Prior to the measurements, all samples were conditioned for a minimum of 5 days at 23°C and 50% relative humidity.

2.3.3 | Quantification of the modes of action

The modes of action of the FRs in the resins and composites were calculated using the techniques already shown in previous studies (see supplementary information).[30–32] The following relevant parameters for these estimations were obtained from the cone calorimetry measurements: peak heat release rate (PHRR), total heat evolved (THE), EHC, and total mass loss (m). All the modes of action calculations use the resin system E90InSi2APP8 as the baseline.

3 | RESULTS AND DISCUSSION

3.1 | Processability of the FR resin formulations

3.1.1 | Rheological properties of the resins and composites

The curves of the complex viscosity of the resins versus temperature are depicted in Figure 2a. The sample E100 shows a decrease in viscosity within the temperature
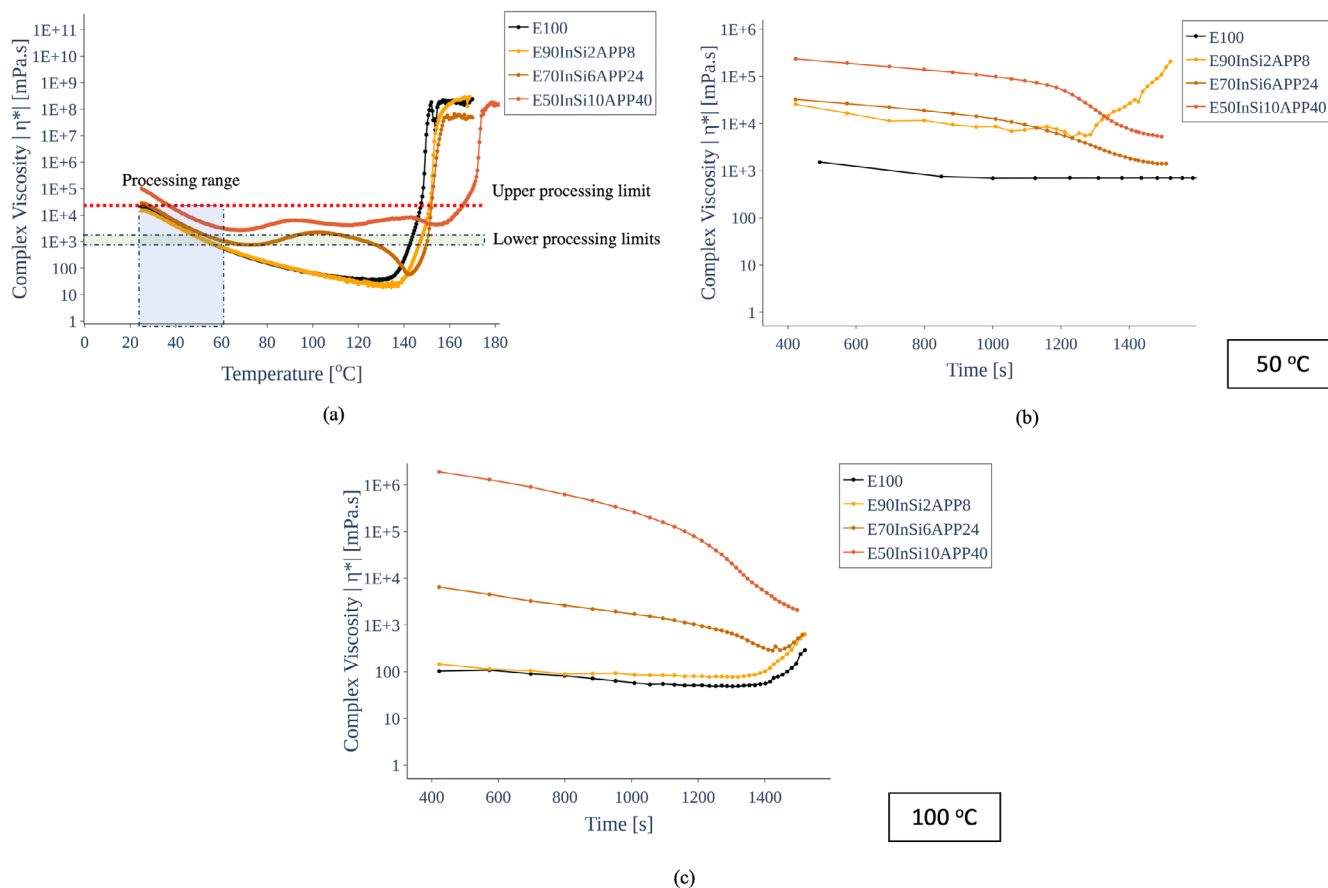

FIGURE 2 Complex viscosity versus temperature (a), and complex viscosity versus time curves (b, c) of various formulations in DGEBA resins with and without FRs. DGEBA, diglycidyl ether of bisphenol A; FR, flame retardant. [Color figure can be viewed at wileyonlinelibrary.com]

range between 25 and 140°C, typical of thermosetting resins,[37] followed by a sharp increase after this point indicating gelation and curing onset. The curve for the E90InSi2APP8 formulation exhibits a similar trend, with a slight decrease in the initial viscosity, possibly due to the plasticizing effect of the additives, and a comparable sharp rise during curing around 140°C, suggesting minimal impact on cure kinetics at this additive concentration. The increase in initial viscosity at room temperature seen in the curves for the E70InSi6APP24 and E50InSi10APP40 formulations compared to E100 indicates that the higher loading of the FRs contribute to a higher viscosity at lower temperatures. This suggests that the additives increase the stiffness of the system and lead to interactions that restrict the flow of the resin.[38] The subsequent decrease in viscosity with temperature indicates a typical shear-thinning behavior[37,39] while the pronounced increase at higher temperatures marks the gelation and curing of the resin, which occurs at a higher temperature for E50InSi10APP40 than E100 as summarized in Figure 4a. The shift to higher temperatures for the start of the viscosity increase indicates that more thermal energy is required to initiate the curing process, which could be due to the additives' influence on the crosslinking mechanism or their stabilizing effect on the resin matrix,[40] preventing the crosslinking from initiating at lower temperatures. In the temperature ranges between 80 and 120°C, it is seen that there is a gradual rise followed by a plateau for the complex viscosities of E70InSi6APP24 and E50InSi10APP40 which points to potential interparticular interactions of the FRs within the resins, particle–matrix interactions, or hydrodynamic effects at these temperatures. Although the viscosity of the resin with lower additive content at 10% w/w contrastingly and steadily falls with increasing temperature, these interactions appear to offset the reduction in viscosity until a critical temperature is reached where the onset of curing reactions dominate.

Based on the processing windows depicted in Figure 2a, the chosen prepreg processing temperatures for the BD GFs are enumerated in Table 2. The frequency sweep curves at 50°C show that E100 remains stable over the measurement range, whereas for the formulations with FRs, the viscosity gently decreases for E70InSi6APP24 and E50InSi10APP40 until ∼1200 s, whereas the viscosity plateaus for E90InSi2APP8 across the measured time range. This is followed by a gradual increase in the viscosity for E90InSi2APP8 and a pronounced decrease for E50InSi10APP40, in the complex viscosity until 1400 s, suggesting that a 50% w/w loading of FRs caused interactions with the EP matrix even at a lower temperature. At 100°, all formulations, including E100, show a decrease in viscosity initially, reflecting typical shear-thinning behavior.[37]

TABLE 2 Summary of the processing temperatures selected for the prepreg line sections from the temperature sweep rheology profile of the various resin formulations.

Resin formulation	Inlet temperature (°C)	Coating unit temperature (°C)	Calendar temperature (°C)
E100	25	40	50
E90InSi2APP8	25	40	50
E70InSi6APP24	40	50	60
E50InSi10APP40	40	50	60

However, after ∼1300 s, there is a clear increase in viscosity for all samples other than E50InSi10APP40, which is much more pronounced than at 50°C. This is indicative of the curing process being initiated more actively at this elevated temperature for all formulations except the highly filled system, which was chosen as the first heating ramp for the resin curing process. The formulations with additives show a delayed onset of this viscosity increase, and the sample with 50% loading of APP + InSi shows a decrease, which suggests that the additives may be interfering with the curing process, potentially due to their interaction with the curing agent or the EP matrix.[40]

3.1.2 | Curing parameters of the resins and composites

Figure 3a,b represent the DSC curves of the first heating cycles of the resins and composites with BD GFs containing increasing amounts of APP + InSi in the DGEBA matrix cured with DICY and Urone. Considering first the curing behavior of the resins, E100 (DGEBA with DICY + UR400) shows a sharp exothermic peak just below 145°C, indicating that the resin is undergoing its primary curing reaction, where the crosslinking between EP groups and the curing agent occurs.

The sharpness of this peak suggests a rapid and efficient cure reaction. In comparison, E90InSi2APP8 exhibits a significant exothermic peak starting just below 150°C and peaking before 160°C. The exothermic peak here, which is less pronounced than in the E100 sample, suggests that the presence of additives slightly delays the curing process or alters the reaction mechanism. E70InSi6APP24 shows a broader and less intense exothermic peak slightly above 150°C. The broader nature of this peak indicates a more gradual curing reaction, which is attributed to the increased percentage of the APP + InSi mixture, which interacts with the curing process, potentially by complexing with the curing agent or by affecting the mobility of the reactive species.
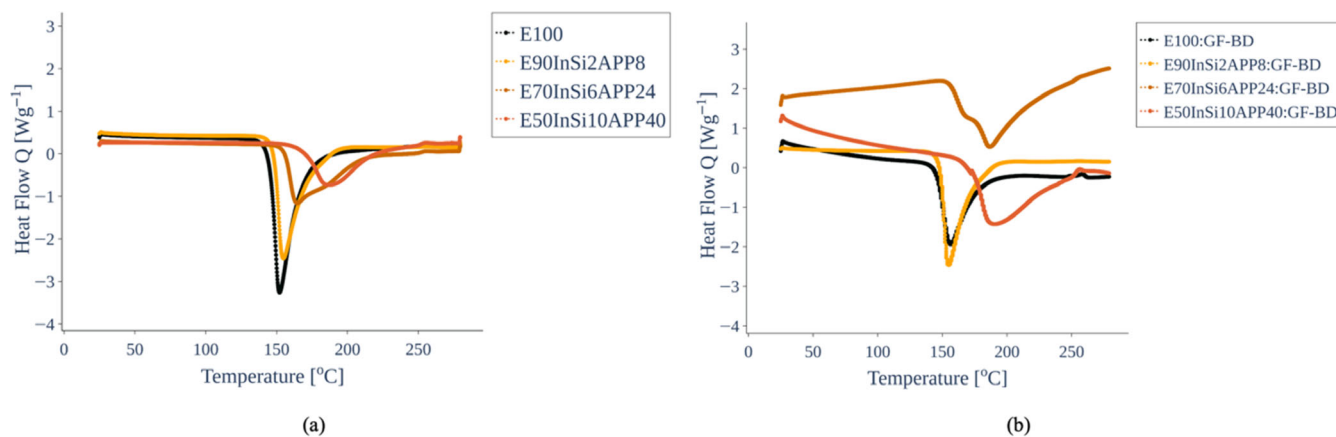
FIGURE 3 DSC curves of the resins (a) and composites (b) containing varying amounts of the FRs. DSC, differential scanning calorimetry; FRs, flame retardants. [Color figure can be viewed at wileyonlinelibrary.com]

E50InSi10APP40, which depicts the curve with the highest level of APP + InSi content at 50% w/w exhibits a very broad exothermic peak at approximately 180°C, which is significantly different from the E100 baseline. The broad and gentle nature of these transitions suggests that the high concentration of additives has a moderate impact on the resin's curing behavior, likely by interfering with the crosslinking process or by changing the chemical environment in which the reaction takes place. For all the formulations, the additives, APP and InSi clearly influence the cure kinetics, as seen by the changes in the shape and intensity of the exothermic peaks compared to the unreinforced EP (E100). The reference composite (E100:GF-BD) with unreinforced DGEBA resin shows minimal endothermic activity, suggesting a low presence of volatiles or moisture, and a subdued exothermic peak, which indicates that the curing reaction is somewhat restrained by the presence of GFs. With increasing amounts of APP and InSi, the exothermic peaks become broader and less intense, indicating that the additives significantly affect the cure kinetics. In the E90InSi2APP8:GF-BD composite, this suggests a delay in the curing mechanism, while in the E70InSi6APP24:GF-BD and E50InSi10APP40:GF-BD composites, the substantial broadening and reduction in intensity of the exothermic peaks suggest that the high level of additives may be impeding the curing process. The interaction between the resin matrix, GFs, and additives leads to a complex interplay affecting the composite's thermal behavior, with the GFs potentially providing a barrier to heat flow. As depicted by the increased onset and peak curing temperatures in Figure 3a,b, the additives seem to slow down the curing reaction in both the resins and composites and alter the thermal behavior of the curing process with increasing content. However, these changes are less significant compared to formulations where the

FRs are chemically reacted with the structure of DGEBA[41–43] and are in the range for the curing behavior of DGEBA/DICY systems in previous studies.[44]

The curing parameters as well as the gel points of the resins and composites are summarized in Figure 4 and Table 3. Additionally, the increase in the FR content causes a linear increase in the curing enthalpy of the resins as depicted in Figure 4c indicating the decreasing exothermicity of the reactions due the presence of the FRs, which act as heat sinks. This change is less distinguishable in the case of the composites as shown in Figure 4d due to the dominance of the GF content at ~70% w/w. The high GF content in the composites dilutes the concentration of reactive resin components. This directly lowers the exothermic potential of the composite compared to the resins by ~150 J/g. Although the curing enthalpy slightly increases with FR content up to 30% w/w in the resin in comparison to the composite without FRs, the enthalpy decreases at 50% FR content in the resin. This can be related to inhomogeneities in the distribution of the FRs at 50% loading causing inhomogeneous fiber-matrix-filler interactions during curing. This is further illustrated in the SEM images in Figure 8.

3.1.3 | Temperature-based mechanics of the resins and composites

Figure 5 depicts the storage modulus G' versus temperature (a) and tan ∂ versus temperature (b) with varying amounts of the FRs up to a temperature of 220°C. E100 exhibits the lowest storage modulus at 30°C with a value of ~1 MPa, suggesting higher chain mobility at lower temperatures. As the temperature rises and approaches the glass transition temperature T_g, G' decreases gently indicating the transition from a glassy to a rubbery state.
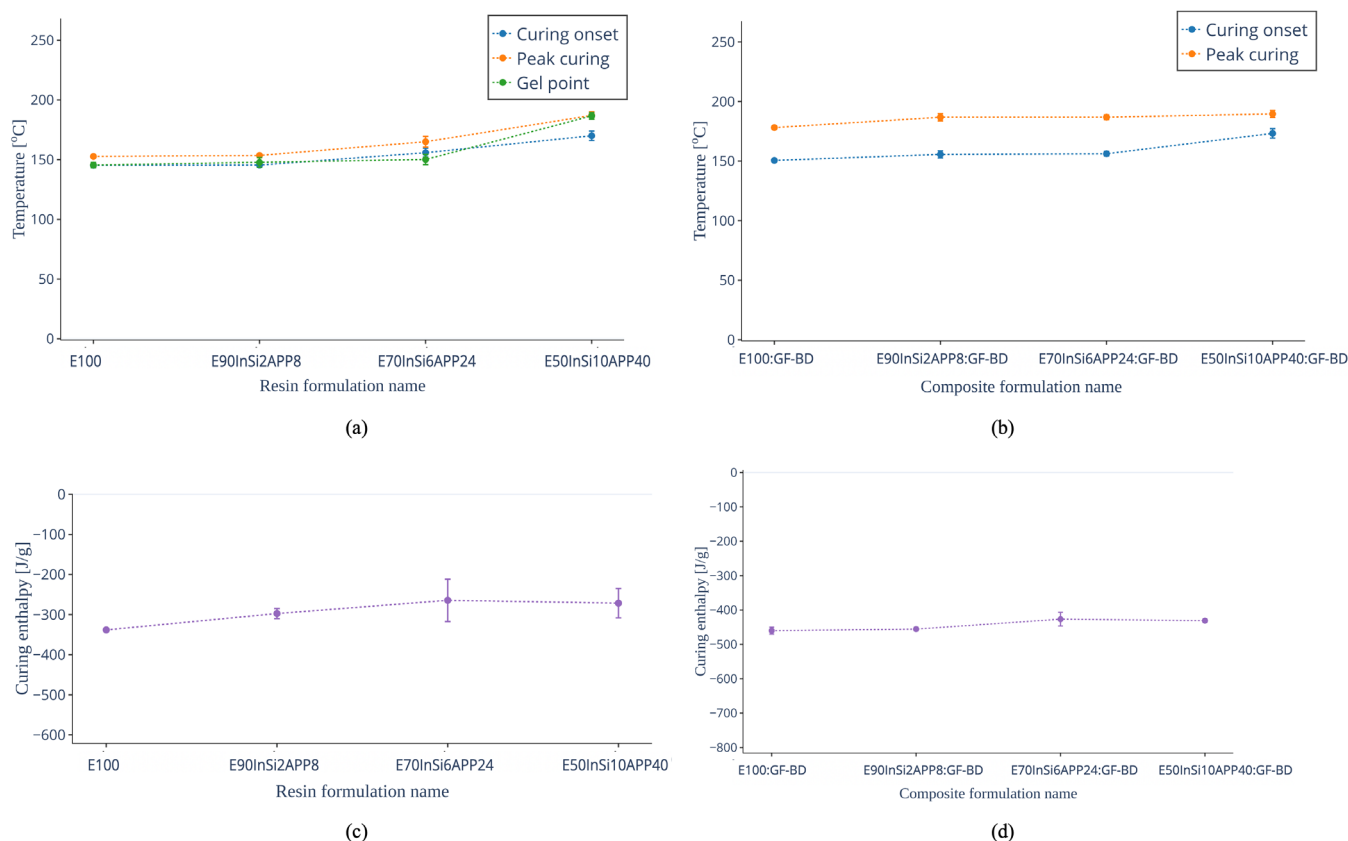
FIGURE 4 Summary of the gel point, peak curing temperature, and curing enthalpies of the resins (a, c) and the composites (b, d). [Color figure can be viewed at wileyonlinelibrary.com]

TABLE 3 Summary of the curing properties of the resin and BD composite formulations with increasing FR content.

Sample	Gel point (°C)	Curing onset (°C)	Peak curing (°C)	Curing enthalpy (J/g)
E100	145.41 ± 0.5	145 ± 0.4	153 ± 1.0	−341 ± 4.0
E90InSi2APP8	147.62 ± 1.0	145 ± 4.0	154 ± 3.0	−297 ± 37.0
E70InSi6APP24	150.11 ± 2.5	156 ± 3.0	165 ± 3.0	−248 ± 5.0
E50InSi10APP40	186.65 ± 1.0	170 ± 5.0	187 ± 4.0	−176 ± 4.0
E100:GF-BD	-	150.52 ± 1.0	178.18 ± 1.5	−460.20 ± 10.0
E90InSi2APP8:GF-BD	-	155.61 ± 3.0	186.80 ± 3.0	−455.67 ± 5.0
E70InSi6APP24:GF-BD	-	156.16 ± 2.0	186.80 ± 3.0	−426.70 ± 20.0
E50InSi10APP40:GF-BD	-	173.26 ± 4.0	189.60 ± 2.0	−431.00 ± 5.0

Abbreviations: BD, bidirectional; FR, flame retardant.

After the T_g, a sharp decline in the storage modulus is evident for all samples. On the other hand, the formulations with additives (E90InSi2APP8, E70InSi6APP24, E50InSi10APP40), demonstrate higher initial moduli of ~1.5, 2, and 2.5 MPa, respectively. Thus, the increased quantity of additives enhances the stiffness of the composite. The thermal response of these materials is further marked by a smooth decrease in modulus with rising temperature, showcasing a strong network at lower temperatures that gradually softens upon heating. Similarly, the tan ∂ curves of the resins show that an increase in FR content leads to lower initial damping factors and shifts the glass transition to lower temperatures, while broadening the T_g peak. This suggests that the higher FR content at 30 and 50% w/w may introduce more complex or less efficient network structures within the resin, leading to increased energy dissipation and affecting the material's thermal behavior. Thus, the FRs not only
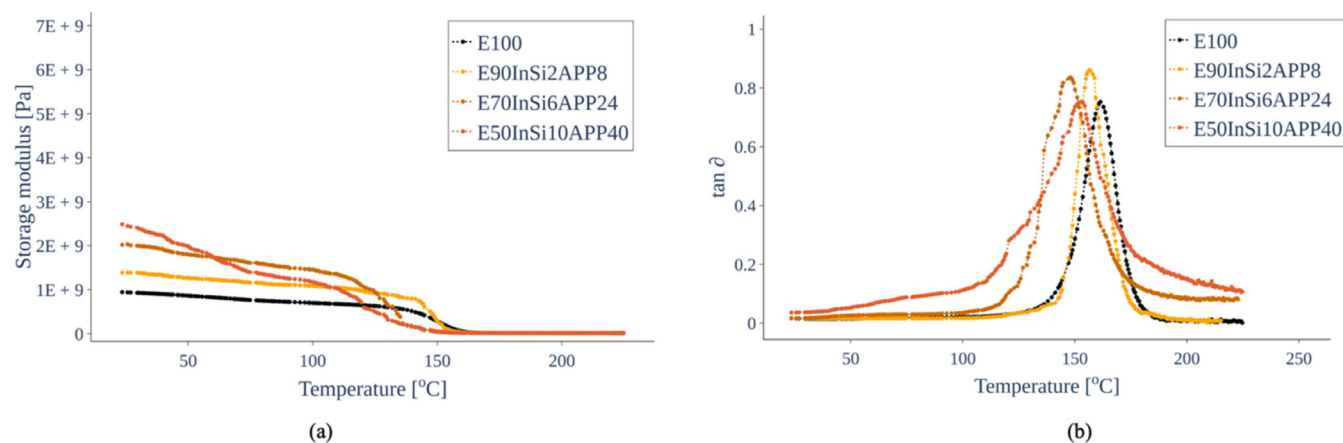
FIGURE 5 DMTA curves of the resins depicting the storage modulus G' versus temperature (a) and tan ∂ versus temperature (b) with varying amounts of the FRs. DMTA, dynamic mechanical thermal analysis; FR, flame retardant. [Color figure can be viewed at wileyonlinelibrary.com]
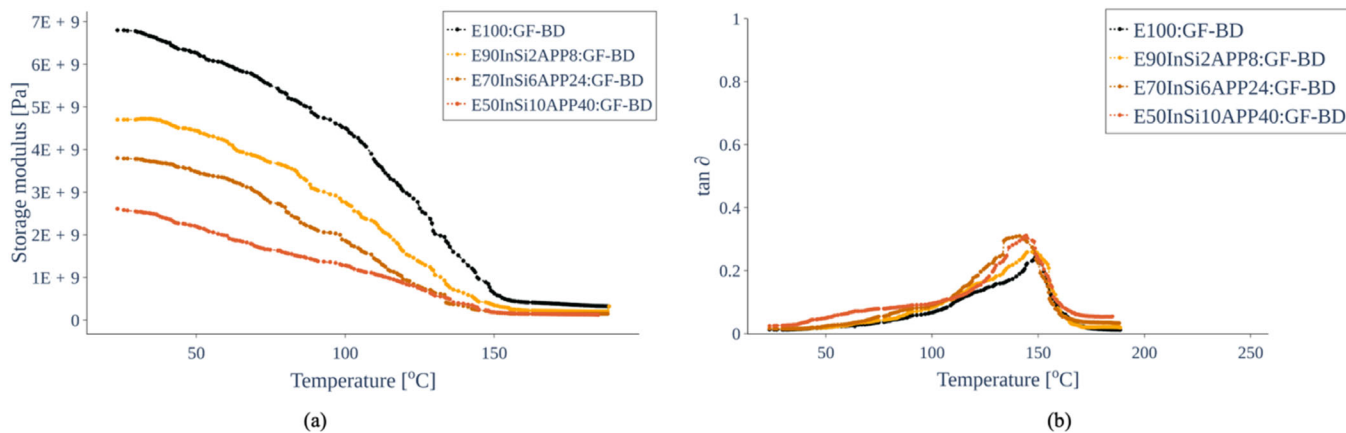

FIGURE 6 DMTA curves of the BD composites depicting the storage modulus G' versus temperature (a) and tan ∂ versus temperature (b) with varying amounts of the FRs. BD, bidirectional; DMTA, dynamic mechanical thermal analysis; FR, flame retardant. [Color figure can be viewed at wileyonlinelibrary.com]

increase the initial stiffness but additionally affect the thermal behavior of the EP resin, altering the T_g by ~10°C for 30% and 50% w/w loading of the FRs as shown in Figure 7. This is, however, negligible compared to formulations containing chemically grafted 9,10-dihydro-9-oxa-10-phosphaphenanthrene-10-oxide (DOPO). For instance, Häublein et al. investigated DOPO with varying P content up to 4% in a Novolac EP resin and found that the increase in P content reduced the T_g to almost 50% that of the unmodified resin.[20]

As shown in Figure 6, transfer of the EP resin formulations to GFRCs leads to an increase in the initial storage modulus for all composites, reflecting the stiffening effect of the fibers. However, within the composites, with increasing FR content a significant decrease in the
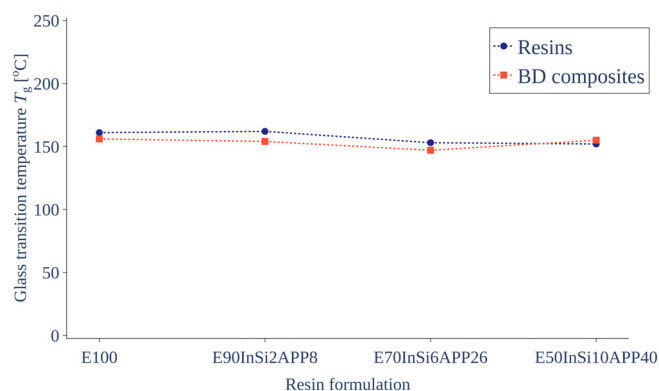

FIGURE 7 Summary of the T_g of the various resins and composite formulations. [Color figure can be viewed at wileyonlinelibrary.com]

initial value of G' occurs from $\sim$7 MPa for E100 to 3 MPa for E50InSi10APP40:GF-BD. The transition region where the modulus drops, appears to be broader compared to the resin, possibly due to the matrix-fiber-filler interactions in the composites. Similar to the resins, there is a broadening of the tan ∂ peaks with increasing FR content in the composites. No significant variations in the T_g of the composites was observed as shown in Figure 7 and Table 4. The values for G' and tan ∂ are in the expected range for DGEBA resins and GFRCs considering that the aerial weight of the GFs used was $\sim$600 g/m^2.[45–47]

3.1.4 | Distribution of FRs in the composites

Figure 8 shows the SEM images of the BD GFRCs with increasing APP + InSi content. In the case of Figure 8a showing E100:GF-BD, the fibers are evenly spaced with a clear boundary between the fibers and the resin rich region, suggesting good adhesion and impregnation of the fibers by the resin. In Figure 8b depicting E90InSi2APP8:GF-BD, a few particles of the FRs are visible. However, they are not evenly distributed in the matrix and are sparsely available. Due to the sparse distribution of APP + InSi at 10% loading upon transfer to the composite, the curing parameters are negligibly impacted. It is evident that the distribution of the FRs in the resin rich areas between the GFs improves in homogeneity and availability in the case of E70InSi6APP24:

TABLE 4 Summary of the curing properties of the resin and BD composite formulations with increasing FR content.

Phosphorous content/% wt	Sample	T_g (°C)
0	E100	161 ± 0.4
∼1.0	E90InSi2APP8	162 ± 0.3
∼3.0	E70InSi6APP26	153 ± 0.4
∼4.0	E50InSi10APP40	152 ± 0.7
0	E100:GF-BD	156 ± 0.5
0.1	E90InSi2APP8:GF-BD	154 ± 1.0
1	E70InSi6APP24:GF-BD	147 ± 1.5
∼3	E50InSi10APP40:GF-BD	155 ± 2.0

Abbreviations: BD, bidirectional; FR, flame retardant.

E100:GF-BD (a)   E90InSi2APP8:GF-BD (b)   E70InSi6APP24:GF-BD (c)   E50InSi10APP40:GF-BD (d)

Increasing FR content in composite

FIGURE 8 SEM images of the distribution of the FRs within the BD composites with increasing FR content. BD, bidirectional; FR, flame retardant; SEM, scanning electron microscopy. [Color figure can be viewed at wileyonlinelibrary.com]

TABLE 5 Summary of the UL-94 ratings, related burning rates, LOI and PHRRs of the various resin and composite samples.

Sample	Classification	Burning rate (mm/min)	OI/vol.% (± 0.2)	PHRR (kW/m^2)
E100	HB40	16	21.1	1360 ± 37
E90InSi2APP8	V-0	-	25.7	486 ± 28
E70InSi6APP24	V-0	-	35	197 ± 15
E50InSi10APP40	V-0	-	41	121 ± 10
E100:GF BD	HB40	0	30.9	385 ± 6
E90InSi2APP8:GF BD	HB40	0	36.3	341 ± 9
E70InSi6APP24:GF BD	V-0	-	35.0	230 ± 6
E50InSi10APP40:GF BD	V-0	-	45.1	180 ± 9

Abbreviation: LOI, limited oxygen index; PHRR, peak heat release rate.

GF-BD depicted in Figure 8c. This is reflected in the minimal impact on the curing parameters—the onset and peak of curing are virtually unchanged, and only a
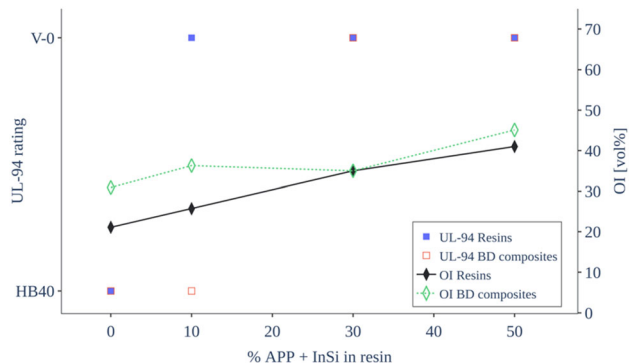

FIGURE 9 Summary of the UL-94 ratings and OIs of the resins and composites with varying APP + InSi content in the resin matrix. APP, ammonium polyphosphate; OIs, oxygen index. [Color figure can be viewed at wileyonlinelibrary.com]

small increase in the curing enthalpy in comparison to the composite without FRs from −460 to −426.70 J/g is observed. In the right-most image Figure 8d depicting E50InSi10APP40:GF-BD, the FR additives are distributed inhomogeneously, both in the intertow and intratow regions causing an increase in the roughness of the sample surface. This causes the increased presence of voids between the GFs. As mentioned previously, the in homogeneities in the distribution of the FRs at 50% loading can cause inhomogeneous fiber-matrix-filler interactions and interfere with the curing process, leading to an increase of ~20°C in the curing onset temperature at the measured ramp rate. This inhomogeneity also causes a break in the trend of increasing curing enthalpy with increasing FR content in the composite and is comparable to that of E70InSi6APP24:GF-BD. It is possible that these particulate materials will act as stress concentrators and initiation points for failure under load, which will be explored in a future investigation.
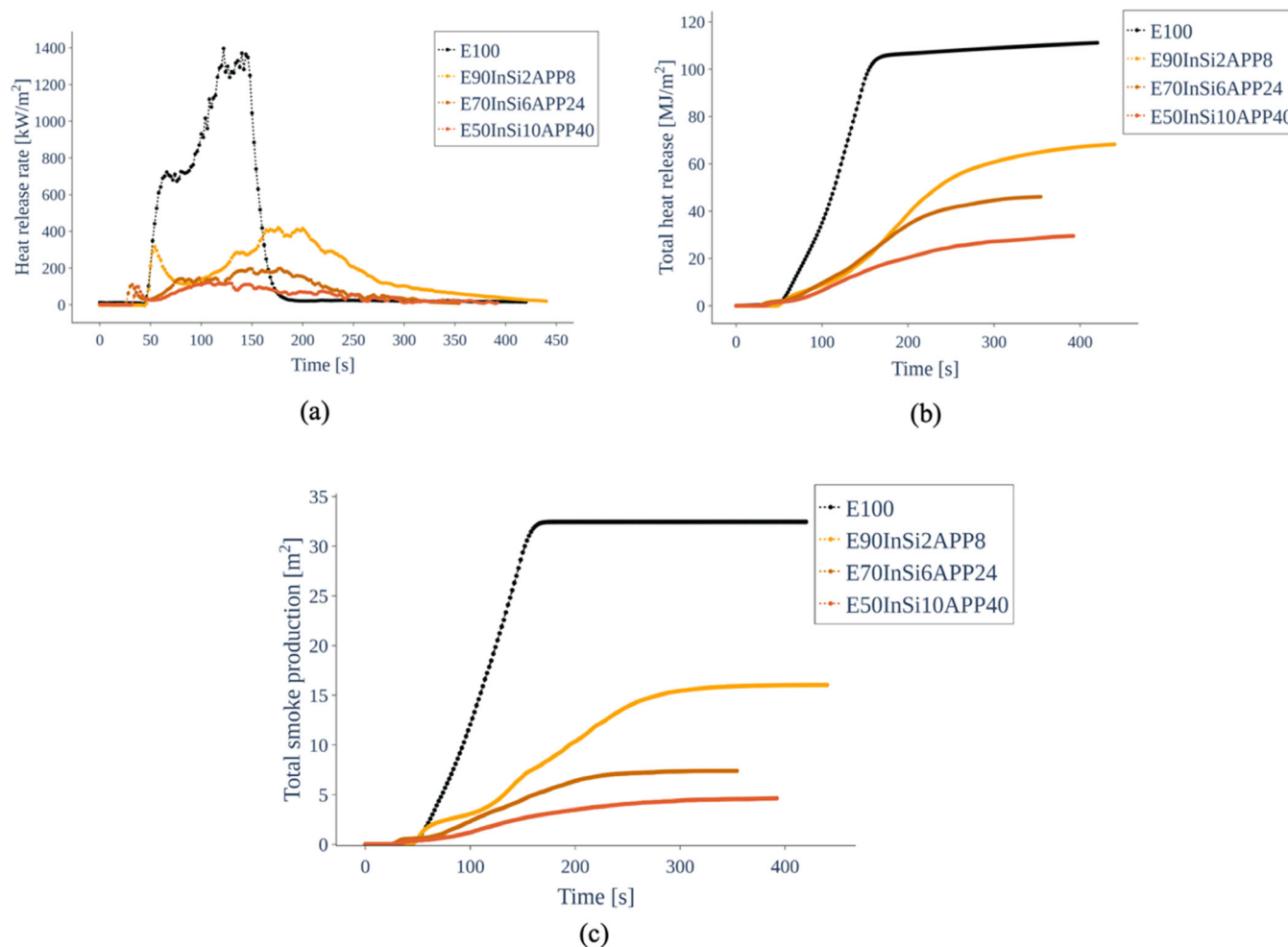

FIGURE 10 Cone calorimetry results for resin formulations with increasing amounts of FRs representing HRR versus time (a), THR versus time (b), and TSP versus time (c). FRs, flame retardants; THR, total heat release; TSP, total smoke production; HRR, heat release rate. [Color figure can be viewed at wileyonlinelibrary.com]

3.2 | Recovering FR action upon transfer to composites

3.2.1 | Flammability testing

From the data in Table 5 and Figure 9, it is evident that the reference samples E100 has a burning rate of 16 mm/min and an oxygen index (OI) of 21.1 vol.%. In comparison, E100:GF-BD has a negligible burning rate despite a rating of HB40 and an increased LOI of 30.9 vol.%. The presence of GFs and binder in the latter increases the OI, suggesting reduced flammability. The resins containing APP + InSi all passed the UL-94 test with a V-0 rating and an increasing LOI with increasing FR content up to 41 vol.%. E90InSi2APP8:GF-BD shows only a rating of HB40 in the composite indicating a potential suppression of the activity of the APP at a loading of 10% w/w in the resin but has a slightly higher LOI in comparison to

E100:GF-BD. The GFs act similar to a candle wick,[28] thus igniting the resin, and lowering the rating due to the suppressed activity of the FRs within. At higher loadings of 30% and 50%, the V-0 rating is recovered indicating a possible recovery of the mode of action of the APP + InSi combination. The LOI increases in a similar trend to that of the resin with higher values for the composites and the resins.

3.3 | Heat and smoke release characteristics

As shown in Figure 10a, the PHRR of the resins containing 10, 30, and 50% w/w of the APP + InSi, significantly decreases by almost to 30% that of E100 over time. However, the resins containing the FRs show a slight reduction in the time to ignition and an extended time to
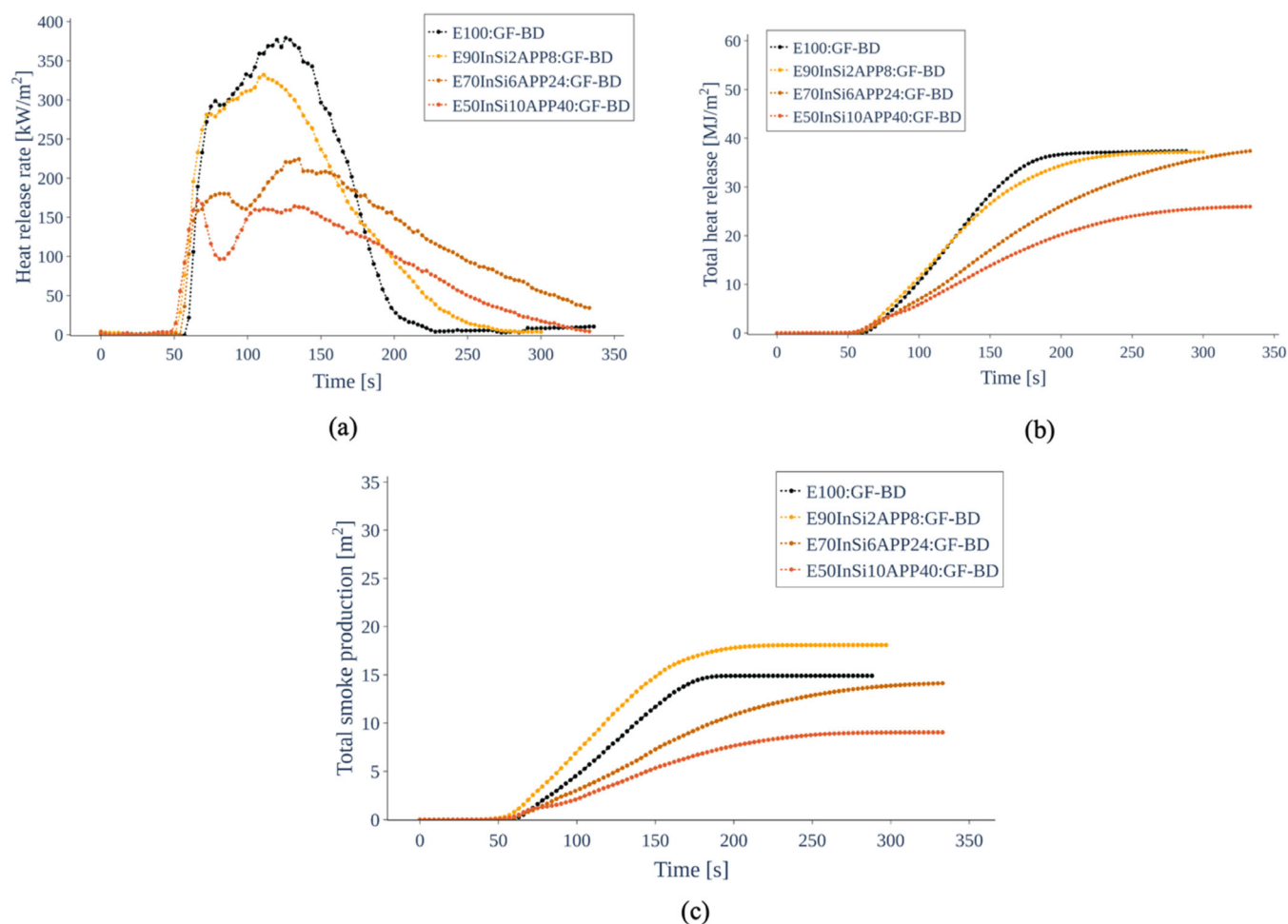
FIGURE 11 Cone calorimetry results for BD composites with different amounts of FRs depicting HRR versus time (a), THR versus time (b), and TSP versus time. (c) Note that the scale of graph (a) is 1/4th that of Figure 10a and that the scale of the graph (b) is half that of Figure 10b. BD, bidirectional; FRs, flame retardants; THR, total heat release; TSP, total smoke production; HRR, heat release rate. [Color figure can be viewed at wileyonlinelibrary.com]

extinction. The PHRR is lowest for E50InSi10APP40, albeit being only slightly lower than that of E90InSi2APP8. The HRR curve of the FR systems presents two broad bands, which is typical for intumescent materials. The initial spike represents an ignition and flame propagation on the surface of the material followed by a constant HRR due to protection by the intumescent char layer. The second increase in the curve is explained by the destruction of the intumescent carbonaceous structure.[48] Similarly, a decline is seen in the maximum value of total heat release (THR) from $\sim$110 to $\sim$70 MJ/m^2, $\sim$ 46 and 30 MJ/m^2 for E100, and the increasing FR contents of 10%, 30%, and 50%, respectively. Additionally, a promising decline in the total smoke production (TSP) occurs with increasing FR content as shown in Figure 10c from $\sim$30 m^2 for E100 to $\sim$4 m^2 for the resin with 50% w/w APP + InSi content.

In the composites (Figure 11a–c) the PHRR decreases due to the presence of the inert GFs at $\sim$70% w/w in the composite compared to the resin E100 to just 30% of the value for E100:GF-BD. The PHRR of E90InSi2APP8:GF-BD at 400 kW/m^2 is just 25% of the value of the resin. Further, with values of the PHRR at $\sim$230 kW/m^2 and 180 kW/m^2 for E70InSi6APP24:GF-BD and E50InSi10APP40:GF-BD, respectively, these are just 18% and 13% of the values of the resin E100. The maximum value of the THR for significantly reduces from $\sim$100 MJ/m^2 for E100 to 40 MJ/m^2 for E100:GF-BD. In the case of the formulations with FRs, the highest THR values of the composites are approximately 50% that of the resin. The TSP of E90InSi2APP8:GF-BD is slightly higher than that of E100:GF-BD indicating a suppressed mode of action of APP and InSi in the composite compared to the resins, which have a similar TSP value. Further, there is a slight increase in the case of E70InSi6APP24:GF-BD and E50InSi10APP40:GF-BD by $\sim$10 and 5 m^2 at 250°C, respectively. These phenomena are further quantified using mode of action estimations in the following section.
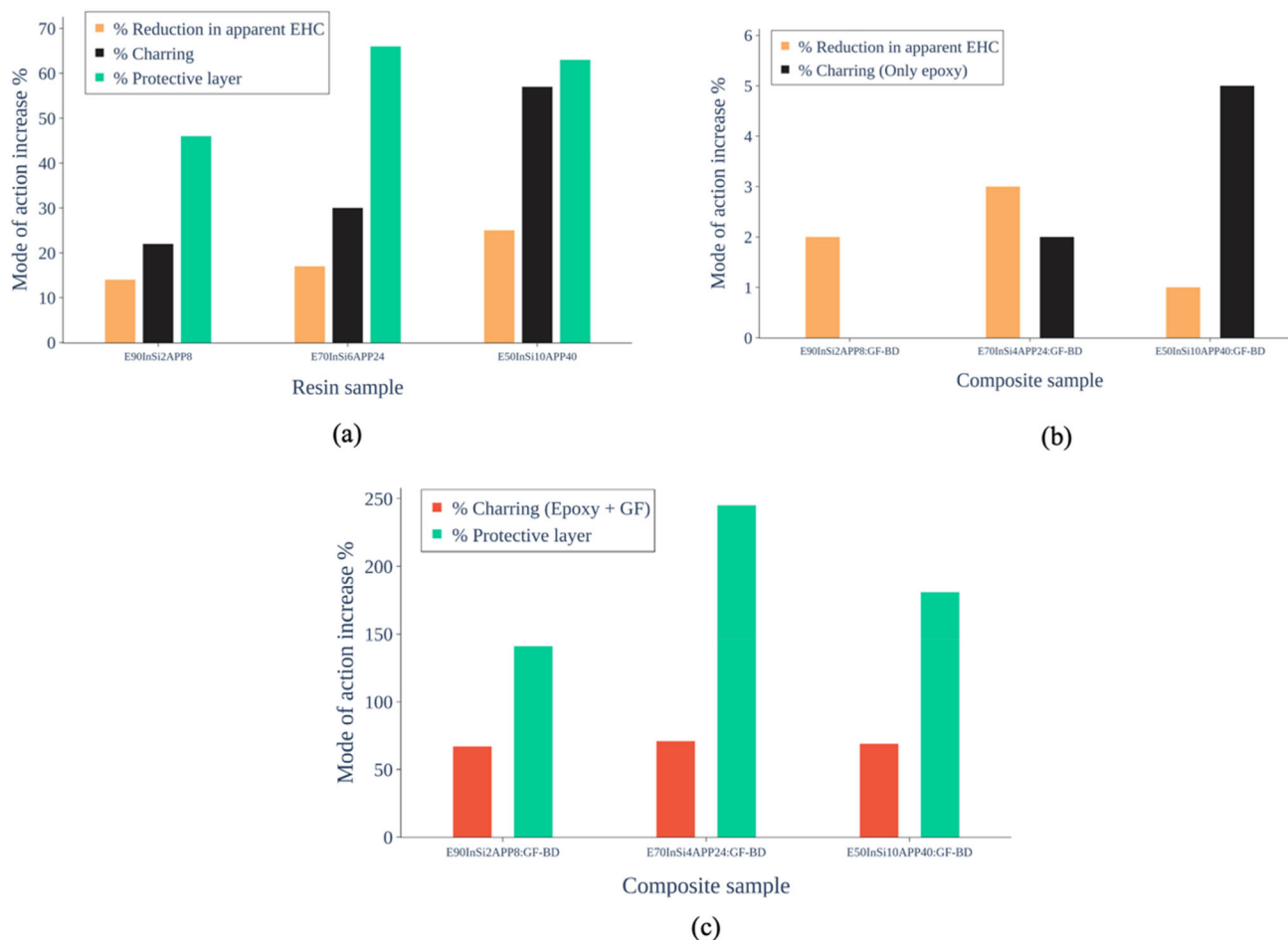

FIGURE 12 Mode of action estimations for the resins (a) and the composites. (b, c) Note the scales of (a–c) are intentionally differentiated to improve the resolution of the data points. [Color figure can be viewed at wileyonlinelibrary.com]
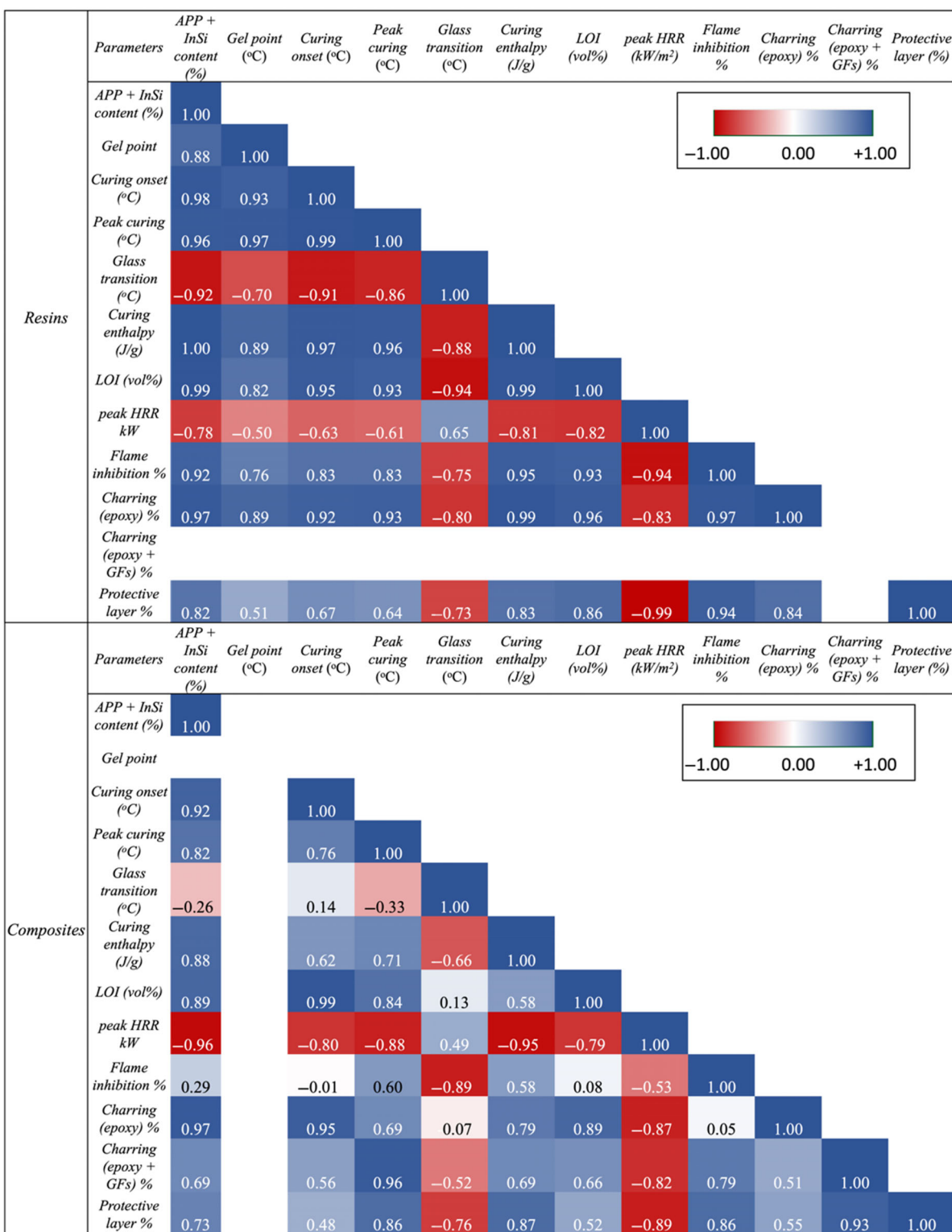
Resins

Parameters	APP + InSi content (%)	Gel point (°C)	Curing onset (°C)	Peak curing (°C)	Glass transition (°C)	Curing enthalpy (J/g)	LOI (vol%)	peak HRR (kW/m²)	Flame inhibition %	Charring (epoxy) %	Charring (epoxy + GFs) %	Protective layer (%)
APP + InSi content (%)	1.00											
Gel point (°C)	0.88	1.00										
Curing onset (°C)	0.98	0.93	1.00									
Peak curing (°C)	0.96	0.97	0.99	1.00								
Glass transition (°C)	−0.92	−0.70	−0.91	−0.86	1.00							
Curing enthalpy (J/g)	1.00	0.89	0.97	0.96	−0.88	1.00						
LOI (vol%)	0.99	0.82	0.95	0.93	−0.94	0.99	1.00					
peak HRR kW	−0.78	−0.50	−0.63	−0.61	0.65	−0.81	−0.82	1.00				
Flame inhibition %	0.92	0.76	0.83	0.83	−0.75	0.95	0.93	−0.94	1.00			
Charring (epoxy) %	0.97	0.89	0.92	0.93	−0.80	0.99	0.96	−0.83	0.97	1.00		
Charring (epoxy + GFs) %												
Protective layer %	0.82	0.51	0.67	0.64	−0.73	0.83	0.86	−0.99	0.94	0.84		1.00

Composites

Parameters	APP + InSi content (%)	Gel point (°C)	Curing onset (°C)	Peak curing (°C)	Glass transition (°C)	Curing enthalpy (J/g)	LOI (vol%)	peak HRR (kW/m²)	Flame inhibition %	Charring (epoxy) %	Charring (epoxy + GFs) %	Protective layer (%)
APP + InSi content (%)	1.00											
Gel point (°C)												
Curing onset (°C)	0.92		1.00									
Peak curing (°C)	0.82		0.76	1.00								
Glass transition (°C)	−0.26		0.14	−0.33	1.00							
Curing enthalpy (J/g)	0.88		0.62	0.71	−0.66	1.00						
LOI (vol%)	0.89		0.99	0.84	0.13	0.58	1.00					
peak HRR kW	−0.96		−0.80	−0.88	0.49	−0.95	−0.79	1.00				
Flame inhibition %	0.29		−0.01	0.60	−0.89	0.58	0.08	−0.53	1.00			
Charring (epoxy) %	0.97		0.95	0.69	0.07	0.79	0.89	−0.87	0.05	1.00		
Charring (epoxy + GFs) %	0.69		0.56	0.96	−0.52	0.69	0.66	−0.82	0.79	0.51	1.00	
Protective layer %	0.73		0.48	0.86	−0.76	0.87	0.52	−0.89	0.86	0.55	0.93	1.00

FIGURE 13 Correlation grid for the various parameters relevant for the resin and composite systems with varying FR contents investigated. FR, flame retardant. [Color figure can be viewed at wileyonlinelibrary.com]

3.3.1 | A comparison of the modes of FR action in the resins and composites

Figure 12a,b shows the modes of action estimates for the resins and composites related to the reduction in the apparent EHC, charring and protective layer formation with all modes compared to the resin system E90InSi2APP8. It is evident that when comparing the activity of APP + InSi in the resin to the composite, the reduction in the apparent EHC (r-EHC) is reduced by

~10% and that the charring behavior of the resin is completely suppressed. All percent values depicted in the graphs are compared to values *f* or the resin system E90InSi2APP8. Within the resins, the r-EHC of APP + InSi increases gradually from 14% to 17% and 25% for 10%, 30%, and 50% w/w loading of the FRs. The r-EHC is highest for E70InSi6APP24:GF-BD at 3%, which is however significantly decreased from the resin. This can be attributed to the release of P-based species, fuel dilution due to the release of NH_3, a change in the combustion efficiency of the flame or a combined result of these effects. Although the charring behavior in the composites is suppressed for E90InSi2APP8:GF-BD, there is a recovery of the behavior in EP for E70InSi6APP24:GF-BD with a value of 2%. When considering the composites as a whole (EP + GFs), there is a significant jump in the residue formation to ~70% for all the formulations. A noticeable increase in the protective layer behavior which can be attributed to the GFs can be seen with values of 141%, 245%, and 181% for E90InSi2APP8:GF-BD, E70InSi6APP24:GF-BD, and E50InSi10APP40:GF-BD, respectively, compared to their resin counterparts with values of 46%, 63%, and 66%. Thus, an increase in the FR content not only improves the gas phase and condensed phase mode of action in the resins, but leads to the recovery of the charring action in the composites. It is evident that the loading of the FRs at 30% is sufficient for the recovery of the charring behavior and protective layer mechanisms in the composite and that an increased loading up to 50% does not confer significant additional advantages. In fact, the protective layer mechanism is optimal for the composite with 30% loading of APP + InSi in the resin.

3.4 | Correlation of parameters in the investigation

A summary of the correlations between the parameters studied in this paper is reported in Figure 13.

A strong positive correlation between the FR content in the resin, and an increase in the curing temperatures is evident, with a strong positive correlation between FR content and curing enthalpy indicating decreasing exothermicity. The curing enthalpy is strongly positively correlated with the heat release characteristics and increasing LOI. Additionally, the strong negative correlation with the glass transition temperature (T_g) and the FR content is supported by a strong negative correlation between the T_g and the LOI. Charring is the most significant mode of action increase that occurs with the increase in FR content, followed by the r-EHC and protective layer behavior. In the composites, unlike the

resins there is no correlation between the FR content and the T_g, and the curing temperatures are only moderately correlated. This implies that the transfer of the resins to the composites causes complex resin-matrix-fiber interactions that vary the thermal behavior of the systems.

Similar to the resins, an increase in the FR content in the resin matrix is strongly negatively correlated with the PHRR obtained via cone calorimetry measurements. The FR content was strongly correlated with an increase in the charring mechanism due to the EP resin in the composite. However, unlike in the resin, there were only moderate correlations between FR loading, the r-EHC and protective layer mechanisms in the composite. This indicates a continued suppression of the same upon transfer to the composites despite increasing FR content. Thus, the premise that tailoring the FR mechanisms in the resin would directly translate upon transfer to the composite must be challenged and systematically investigated to avoid loss of flame retardancy behavior.

4 | CONCLUSION

This research investigates the processibility and flame retardancy of DGEBA EP resins, filled with APP and InSi at 10%, 30%, and 50% by weight, for transfer to BD GFRCs using prepregs. The study assesses resin viscosity, cure kinetics, and thermal stability through rheometry, DSC, and DMTA. SEM imaging is used to evaluate the distribution of FRs in the matrix. The flammability of the composites is analyzed using UL-94, LOI tests and cone calorimetry, with particular emphasis on the PHRR, THR, and TSP. Although all the resin formulations containing the FRs achieved a V-0 rating in UL-94 tests, with increasing LOIs with increasing FR content, the composite with 10% FR content in the resin is rated only HB40. This loss of FR efficiency is mirrored in the mode of action estimations where it was found that the charring mode of action was completely suppressed in the composite with 10% FR content. A 30% concentration of the FRs in the resin was found to be adequate to not only restore the charring action in the composite but produces an optimized protective layer mechanism in the composite. It was found that the distribution of the FRs is more homogenous in the resin rich regions of the composite with a 30% loading of the FRs, and an additional increase to 50% w/w in the resin increased presence of voids between the GFs. It is however possible, that these FRs act as stress concentrators and initiation points for failure under load, which makes studying the potential trade-offs between fire performance and mechanical behavior vital. This behavior will be investigated in a future study.

AUTHOR CONTRIBUTIONS

Sruthi Sunder: Conceptualization (lead); data curation (equal); formal analysis (equal); investigation (equal); validation (equal); visualization (lead); writing – original draft (lead). **Maria Jauregui Rozo:** Conceptualization (equal); data curation (equal); formal analysis (equal); investigation (equal); methodology (equal); writing – original draft (equal). **Sneha Inasu:** Formal analysis (equal); investigation (equal); writing – original draft (supporting). **Bernhard Schartel:** Funding acquisition (equal); project administration (equal); supervision (equal); writing – review and editing (equal). **Holger Ruckdäschel:** Funding acquisition (equal); project administration (equal); supervision (equal); writing – review and editing (equal).

ACKNOWLEDGMENTS

CONFLICT OF INTEREST STATEMENT

The authors declare no competing financial interest or personal relationships that could have appeared to influence the work reported in this paper.

DATA AVAILABILITY STATEMENT

The data from this investigation is available from the authors upon reasonable request.

ORCID

Holger Ruckdäschel https://orcid.org/0000-0001-5985-2628

REFERENCES

[1] M. L. Cain, _Applications and Recent Developments_, Nova Science Publishers, New York **2016**.

[2] A. Somaiah, B. Anjaneya Prasad, N. N. Kishore, _Mater. Today: Proc._ **2022**, _62_, 3226.

[3] S. Zheng, P. A. Lucas, Understanding chemical resistance in epoxy system. **2020**. https://www.rodpub.com/email/cw/Whitepapers/Evonik/3/Evonik_Whitepaper.pdf (accessed January 2024)

[4] A. Kaushik, P. Singh, J. Kaushik, _Int. J. Polym. Mater._ **2006**, _55_, 425.

[5] M. C. S. Ribeiro, C. M. L. Tavares, A. J. M. Ferreira, _J. Polym. Eng._ **2002**, _22_, 27. https://doi.org/10.1515/POLYENG.2002.22.1.27

[6] F. J. Martin, K. R. Price, _J. Appl. Polym. Sci._ **1968**, _12_, 143.

[7] A. Kelly, _Concise Encyclopedia of Composite Materials_, Elsevier, Amsterdam **2012**. https://books.google.com/books?hl=en&lr=&id=Ia6GAAAAQBAJ&oi=fnd&pg=PP1&dq=concise+Encyclopedia+of+Composite+Materials+-+Page+40&ots=0fGQuVoVWf&sig=0f7PwS6-qxHJwMmg4gAhG3f8h1I (accessed January 2024)

[8] P. O. Darnerud, _Environ. Int._ **2003**, _29_, 841.

[9] B. K. Kandola, F. Magnoni, J. R. Ebdon, _J. Vinyl Addit. Technol._ **2022**, _28_, 17.

[10] F. R. Abe, A. Á. S. de Oliveira, R. V. Marino, T. C. R. Rialto, D. P. Oliveira, D. J. Dorta, _Ecotoxicol. Environ. Saf._ **2021**, _208_, 111745.

[11] P. Xiong, X. Yan, Q. Zhu, G. Qu, J. Shi, C. Liao, G. Jiang, _Environ. Sci. Technol._ **2019**, _53_, 13551.

[12] S. Shaw, _Rev. Environ. Health_ **2010**, _25_, 261.

[13] E. D. Weil, S. Levchik, _J. Fire Sci._ **2004**, _22_, 25.

[14] A. A. Klyosov, _Wood-Plastic Composites_, John Wiley & Sons, New Jersey **2007**.

[15] F. Wang, J. Liao, M. Long, L. Yan, M. Cai, _Polymer_ **2023**, _15_, 1304.

[16] P. Khalili, K. Y. Tshai, D. Hui, I. Kong, _Composites, Part B_ **2017**, _114_, 101.

[17] W. P. Lim, M. Mariatti, W. S. Chow, K. T. Mar, _Composites, Part B_ **2012**, _43_, 124.

[18] L. Liu, Y. Zhang, L. Li, Z. Wang, _Polym. Adv. Technol._ **2011**, _22_, 2403.

[19] K. S. Lim, S. T. Bee, L. T. Sin, T. T. Tee, C. T. Ratnam, D. Hui, A. R. Rahmat, _Composites, Part B_ **2016**, _84_, 155.

[20] M. Häublein, K. Peter, G. Bakis, R. Mäkimieni, V. Altstädt, M. Möller, _Materials_ **2019**, _12_, 1528.

[21] W. Liu, Y. T. Pan, J. Zhang, L. Zhang, J. S. Moya, B. Cabal, D. Y. Wang, _Polym. Degrad. Stab._ **2021**, _185_, 109495.

[22] G. M. Wu, B. Schartel, M. Kleemeier, A. Hartwig, _Polym. Eng. Sci._ **2012**, _52_, 507.

[23] X. Zhang, F. Zhang, W. Zhang, X. Tang, H. J. S. Fan, _Colloids Surf., A_ **2021**, _610_, 125917.

[24] Z. B. Shao, J. Zhang, R. K. Jian, C. C. Sun, X. L. Li, D. Y. Wang, _Colloids Surf., A_ **2021**, _149_, 106529.

[25] J. Yang, Y. Hua, J. Sun, X. Wang, X. Gu, S. Zhang, _Adv. Eng. Mater._ **2023**, _25_, 2300011.

[26] M. Rajaei, D. Y. Wang, D. Bhattacharyya, _Composites, Part B_ **2017**, _113_, 381.

[27] A. P. Mouritz, A. G. Gibson, _Fire Properties of Polymer Composite Materials_, Springer Science & Business Media, Berlin **2007**.

[28] X. Chen, C. Wang, S. Liu, A. Zhang, W. Liu, L. Qian, _Polym. Adv. Technol._ **2023**, _34_, 876.

[29] B. Schartel, A. Weiß, F. Mohr, M. Kleemeier, A. Hartwig, U. Braun, _J. Appl. Polym. Sci._ **2010**, _118_, 1134.

[30] S. Rabe, Y. Chuenban, B. Schartel, _Materials_ **2017**, _10_, 455.

[31] Y. Hu, X. Wang, _Flame Retardant Polymeric Materials: A Handbook_, CRC Press, Florida **2019**.

[32] S. Brehme, B. Schartel, J. Goebbels, O. Fischer, D. Pospiech, Y. Bykov, M. Döring, _Polym. Degrad. Stab._ **2011**, _96_, 875.

[33] C. Pawelski-Hoell, S. Bhagwat, V. Altstädt, _Polym. Eng. Sci._ **2019**, _59_, 1840.

[34] S. Sunder, M. Jauregui Rozo, S. Inasu, B. Schartel, H. Ruckdäschel, *Polym. Compos.* **2024**, *45*, 9389.

[35] M. Demleitner, Prepreg Technology at Polymer Engineering. https://www.polymer-engineering.de/wp-content/uploads/2020/12/Prepregs_at_Polymer_Engineering.pdf

[36] B. Schartel, M. Bartholmai, U. Knoll, *Polym. Degrad. Stab.* **2005**, *88*, 540.

[37] P. Moldenaers, R. Keunings, *Theoretical and Applied Rheology: Proceedings of the XIth International Congress on Rheology, Brussels, Belgium, August 17–21*, Elsevier, Amsterdam **1992**. https://books.google.com/books?hl=en&lr=&id=SVMvBQAAQBAJ&oi=fnd&pg=PP1&dq=Theoretical+and+Applied+Rheology:+Proceedings+of+the+XIth+...+-+Page+327&ots=sGaWRtxrhc&sig=wy00arXFcq76JOAyomx3KTaTppk (accessed January 2024)

[38] K. Wattanakul, H. Manuspiya, N. Yanumet, *J. Compos. Mater.* **2011**, *45*, 1967.

[39] R. Meier, C. Kirdar, N. Rudolph, S. Zaremba, K. Drechsler, *AIP Conf. Proc.* **2014**, *1593*, 458.

[40] Y. Zhao, D. Drummer, *Polymer* **2019**, *11*, 1797.

[41] M. Frigione, A. Maffezzoli, P. Finocchiaro, S. Failla, *Adv. Polym. Technol.* **2003**, *22*, 329.

[42] J. Hu, J. Shan, J. Zhao, Z. Tong, *Thermochim. Acta* **2016**, *632*, 56.

[43] Y. Sun, Y. Peng, Y. Zhang, *Polymer* **2022**, *14*, 245.

[44] M. Hayaty, H. Honarkar, M. H. Beheshty, *Iran. Polym. J.* **2013**, *22*, 591.

[45] M. Kimoto, *J. Mater. Sci.* **1990**, *25*, 3327.

[46] I. Khurana, C. Pratap, S. Singh, A. Bansal, R. Butola, *Mater. Today: Proc.* **2020**, *25*, 946.

[47] M. Agrawal, M. Gupta, R. T. Durai Prabhakaran, P. Mahajan, *Polym. Compos.* **2023**, *45*, 28008.

[48] S. Bourbigot, M. Le Bras, R. Delobel, *J. Fire Sci.* **1995**, *13*, 3.

SUPPORTING INFORMATION

Additional supporting information can be found online in the Supporting Information section at the end of this article.